A Force-Controlled Robotic Micromanipulation System for Mechanotransduction Studies of *Drosophila* Larvae

Weize Zhang, Alexandre Sobolevski, Bing Li, Yong Rao, and Xinyu Liu*

***Abstract*— This paper presents an automated robotic micromanipulation system capable of force-controlled mechanical stimulation and fluorescence imaging of *Drosophila* larvae, for mechanotransduction studies of *Drosophila* neural circuitry. An elastomeric microdevice is developed for efficient immobilization of an array of larvae for subsequent force-controlled touching. A microelectromechanical systems (MEMS) based force sensor is integrated into the system for closed-loop force control of larva touching at a resolution of 50 μN. Two microrobots are coordinately servoed using orchestrated position and force control laws for automatic operations. The system performs simultaneous force-controlled larva touching and fluorescence imaging at a speed of 4 larvae per minute, with a success rate of 92.5%. This robotic system will greatly facilitate the dissection of mechanotransduction mechanisms of *Drosophila* larvae at both the molecular and cellular levels.**

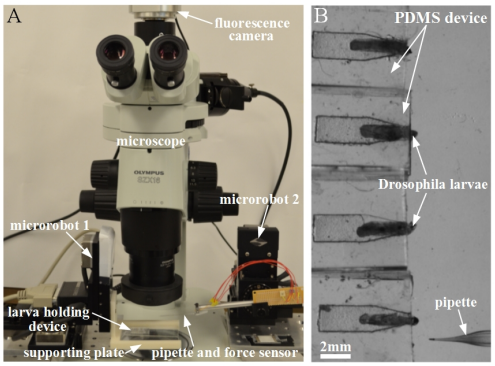

Fig. 1. (A) Robotic micromanipulation system setup. (B) PDMS Larva immobilization device.

I. INTRODUCTION

Robotic micromanipulation of biological samples (e.g., cells, tissues, and organisms) has found important applications in basic biology studies and medical research [1]–[5]. Force sensing and control play critical roles in robotic micromanipulation [6]. Real-time measurements of interaction forces between the end-effector and the biological sample provide additional feedback of the ongoing manipulation, and could improve the dexterity and robustness of the robotic systems. For instance, the detection of indentation forces during cell injection can accurately predict the penetration of cell membranes and thus trigger the subsequent material deposition [7]. Closed-loop control of grasping forces during robotic cell pick-place can guarantee secured grasping while avoiding cell damage by overlarge forces [1].

The capability of accurately regulating interaction forces during robotic micromanipulation is also useful for applying well-controlled mechanical stimuli to living cells or organisms and study their mechanotransduction pathways [8]. *Drosophila* is a popular model organism for mechanobiology studies [9]. A recent study demonstrated that millinewton-level touches at anterior segments of *Drosophila* larvae induced reorientation and selection of a new path for forward movement [10]. Follow-up experiments revealed that a set of ~50 interconnected neurons expressing the cell-surface protein Turtle (Tutl) are involved in the adjustment of moving direction. These findings shed light on the unknown mechanisms controlling navigational behaviors in response to mechanical stimulation, and the further dissection of the Tutl-positive neural circuitry is needed.

Simultaneously performing mechanical stimulation of *Drosophila* larvae and fluorescent calcium imaging of transmissions in Tutl-positive neural circuits will enable the investigation of roles of individual Tutl-positive neurons in regulation of the touch-induced movement adjustment. However, the experimental setup previously employed [10] cannot carry out this type of experiments because it lacks an effective mechanism for immobilizing *Drosophila* larvae for fluorescent imaging. In addition, the gentle touch was applied manually using a fine hair, and inconsistent touch locations and less accurate touch force regulations led to variations in results obtained from different experiments and by different operators. A micromanipulation system capable of high-resolution touch force control and quantitative fluorescent imaging is highly desired.

This paper reports the development of a *Drosophila* larva manipulation system featuring full automation, closed-loop touch force control, batch larva immobilization, and *in-situ* fluorescent imaging during touch stimulation. A microfabricated device is created to securely immobilize an array of larvae for subsequent force-controlled touching and fluorescence imaging, and a MEMS force sensor is integrated into the system for closed-loop force control at a resolution of 50 μN. Two microrobots are coordinately-controlled based on microscopic vision feedback to apply quantitative mechanical stimuli to the immobilized larvae, and touch-induced

This work was supported by National Sciences and Engineering Research Council of Canada, Fonds québécois de la recherche sur la nature et les technologies, and Canadian Research Chairs Program.

Weize Zhang, Alexandre Sobolevski, Bing Li, and Xinyu Liu are with the Biomedical Microsystems Laboratory, McGill University, 817 Sherbrooke Street West, Montreal, QC, Canada, H3A 0C3. xinyu.liu@mcgill.ca. Bing Li is also with the School of Information and Engineering, Huzhou Teachers College, China.

Yong Rao is with the Department of Neurology and Neurosurgery, McGill University.

978-1-4244-7929-0/14/$26.00 ©2014 IEEE

calcium level changes in Tutl-positive neurons are accurately measured via fluorescence imaging. This micromanipulation system is capable of simultaneous mechanical stimulation and fluorescence imaging of *Drosophila* larvae in an accurate and consistent manner, which will enable a wide variety of mechanotransduction studies in *Drosophila*.

II. SYSTEM SETUP AND METHODS

A. Robotic System Setup

As shown in Fig. 1(A). The robotic system employs a stereo fluorescence microscope, two three-degree-of-freedom (3-DOF) micromanipulators (microrobots), a polydimethylsiloxane (PDMS) larva immobilization device carried by microrobot-1 (left), and an assembly of a glass pipette (25 μm tip) and a MEMS piezoresiseive force sensor mounted on microrobot-2 (right). A fluorescence camera is mounted on the microscope for high-resolution fluorescence imaging. A host computer mounted with a motion-control card is used to run the algorithms of force data acquisition, imaging processing, and motion/force control. The MEMS piezoresistive force sensor uses a Wheatstone bridge circuit for converting resistance changes of two piezoresistors on the sensor into voltage signals. The measurement range, resolution and sensitivity of the sensor/pipette assembly was calibrated to be 0-120 mN, 50 μN, and 0.93 mV/mN, respectively.

B. Larva Immobilization Device

Fluorescence imaging of *Drosophila* larvae requires their bodies to be firmly immobilized. To observe Tutl-positive neurons inside a larva body, it is preferred to mechanically compress the larva body to a much smaller thickness so that the fluorescence light could pass the body tissues more efficiently. PDMS microfluidic devices have been applied to *Drosophila* larvae immobilization [11]. However, these devices fixed the larvae in enclosed chambers, and does not allow a pipette to reach the larva body. Here, a simple design was proposed for rapidly immobilizing single larvae with their heads exposed outside the device for touching. Fig. 1(B) shows the PDMS device with four larvae immobilized. It includes four immobilization modules for fixing four third-instar larvae. Each module includes a microchannel fabricated using soft lithography, and the thickness of the microchannel is 130 μm so that the microchannel could firmly compress the larvae body (0.8-1 mm thick) upon bonding with a glass substrate. Each microchannel has a 0.75$\pm$0.08 mm opening, formed via manual blade cutting.

For larva immobilization, a double-sided transparent tape is first attached to the glass substrate, and four larvae are then transferred to the tape using a larva pick. The adhesive tape significantly reduces the larvae locomotion and facilitates the subsequent immobilization. Each immobilization module is manually aligned with a larva and then placed onto the adhesive tape to fix the larva. The adhesion between the tape and the PDMS bottom surface is strong enough to securely immobilize the larva. The four modules are arranged on the substrate to form an array of four fixed larvae with a spacing of 4.5$\pm$0.8 mm. This regular array greatly simplifies the robotic larva positioning task during operation. The PDMS device is reusable after washing and sterilization.

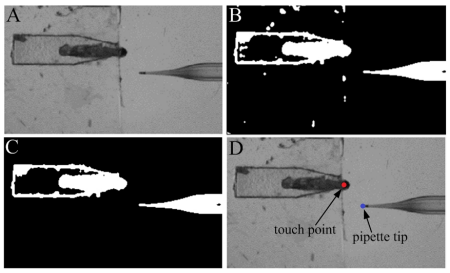

Fig. 2. Image processing sequence of identifying the pipette tip and the touch location on the larva nose.

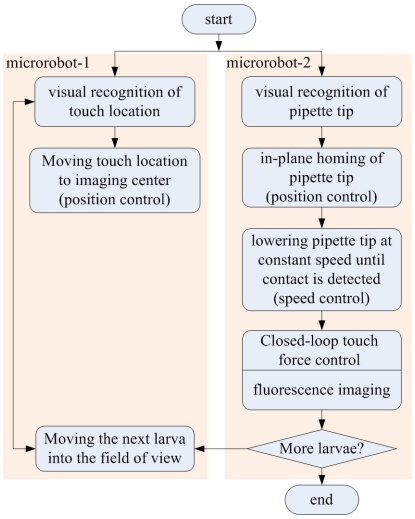

Fig. 3. Overall control sequence of robotic operations.

C. Overall Control Sequence

After immobilization, the PDMS device with larva samples is placed onto the supporting plate of microrobot-1 (Fig. 1(A)), with the first target larva in the field of view of the microscope. The pipette tip is also brought into the field of view. The control sequence, as shown in Fig. 3, starts from visual recognition of image coordinates of the pipette tip and the centroid of the first larva head (target location for touching). The two microrobots are controlled using an image-based, look-then-move architecture (Fig. 4), and closed-loop PID controllers are used to regulate their motions. Coordinate transformations between the image frame and the two microrobot frames are carried out online to determine the microrobot motions based on the image coordinates of target locations. The pipette tip is then moved in-plane to the image coordinate of the larva head centroid, and the microrobot-2 moves the pipette downwards at a constant speed until a contact is detected from the force feedback. The microrobt-2 is then controlled by a PID force controller (Fig. 4) until the desired touch force level is achieved. During touching, fluorescence images were obtained at 10 frame/s. After the first larva is touched, the next one is brought into the field

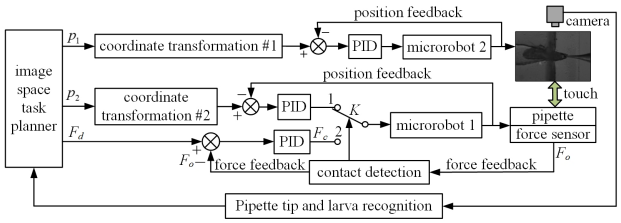

Fig. 4. Schematic diagram of controller.

of view, and the same operation procedure is repeated until all the four larvae are manipulated.

D. Visual Recognition of Pipette Tip and Touch Location

An image processing algorithm is developed to identify the pipette tip and the head of target larva. The original grayscale image (Fig. 2(A)) is first binarized into a black-white image (Fig. 2(B)) using Otu's adaptive thresholding method [12]. Based on the connectivity of the white areas, the two biggest areas, corresponding to the larva (connected with the channel walls) and the pipette, are identified and removed from the image to create a 'background' image that just includes noise features. This 'background' image is subtracted from the original binary image to leave only the two biggest areas (Fig. 2(C)). In the current setup, the pipette area is always smaller than the larva connected with the channel walls. Thus, for the biggest area (larva and channel walls), the image coordinates of rightmost pixel are identified and regarded as the tip of the larva head, and the touch location is set to be the point 400 μm away on the left of the larva head tip (red point in Fig. 2(D)). In the second biggest area (pipette), the image coordinates of the leftmost pixel are found and saved as the pipette tip (blue point in Fig. 2(D)). The vertical coordinate of the pipette tip (in the frame of microrobot-2) is not needed for operation since the force sensor is able to detect the initial contact while lowering the pipette.

E. Touch Force Control

As shown in Fig. 4, the control system includes two PID position controllers for regulating the motions of the two microrobots, and one PID force controller for adjusting the touch force applied to *Drosophila* larvae. Visual feedback is used to provide the microrobots with image coordinates of the pipette tip and the touch location. During automatic operations, an image-based task planner receives real-time visual feedback, plans the motions of two microrobots, and generates reference signals (p_1 and p_2) for the PID position controllers. The motion regulation of microrobot-2 is transited from position control to force control once the initial touch is detected (the virtual switch K is thrown from state 1 to state 2).

The initial contact between the pipette tip and the larva nose is detected by monitoring the force feedback from the MEMS sensor. The force data are sampled at 500 Hz. The derivatives between two adjacent force data points (e.g., force changing speed) are calculated on 100 consecutive data points, and the average of these derivatives is used as a de-noised indicator for the changing speed of the force feedback. For a speed of 100 μm/s at which the pipette is lowered, a threshold of 2.5 mN/s is used to trigger the controller transition.

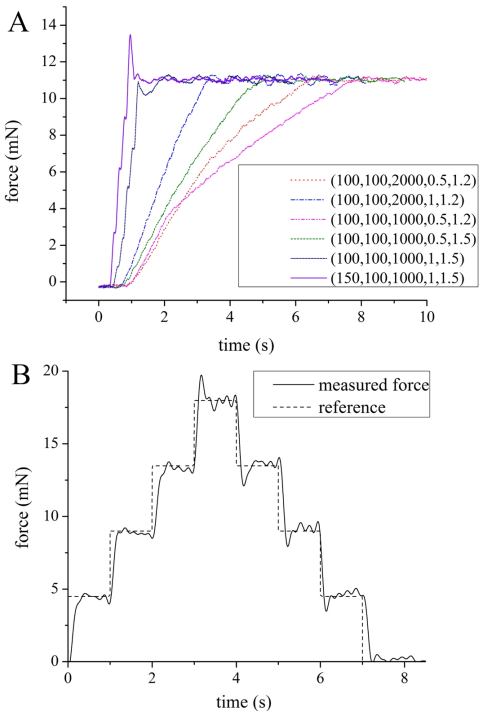

Fig. 5. Step responses of the PID force controller with different combinations of controller parameters (K_p, K_i, K_d, I_{sup}, V_{sup}).

The PID force controller receives the instruction of desired touch force (F_c in Fig. 4) from the task planner, compares it with the force feedback (F_o in Fig. 4), and computes voltage signals as inputs for microrobot-2 based on PID control law. The force controller can be expressed by

$$V_c = K_p e_f(t) + K_i \sum e_f(t) + K_d [e_f(t) - e_f(t-1)] \quad (1)$$

where V_c denotes the voltage control signal for microrobot-2, and $e_f(t) = F_o(t) - F_d$. K_p, K_i, and K_d are the three gains of the PID controller.

III. EXPERIMENTAL RESULTS AND DISCUSSIONS

The larvae used in the experiments were transgenically encoded with green fluorescent proteins (GFP) in Tutl-positive neurons. Third-instar larvae were immobilized in the PDMS device, and the whole immobilization process took less than two minutes. A 3.2× objective (NA=0.15) was used for both bright-field and fluorescence imaging, and the horizontal and vertical pixel sizes were calibrated to be $s_x = s_y = 0.5$ μm.

A. Closed-Loop Force Control

Five parameters of the PID force controller were optimized through extensive trail-and-error experiments. Besides the

three PID gains (K_p, K_i, K_d), the limits of the integration component, I_{sup}, and the limit of the voltage control input of microrobot-2, V_{sup}, were also considered. Two inequalities were implemented in the controller to limit the overshoot magnitudes of the touch force and protect the fragile MEMS force sensor: (i)$|K_i \sum e_v(t)| \leq I_{\text{sup}}$, and (ii) $|V_c| \leq V_{\text{sup}}$.

Based on the results from a previous study [10], the touch force for larva stimulation was controlled in the range of 1-10 mN. Fig. 5(A) shows the experimental results of the step response curves of the PID controller at different combinations of the five parameters. The combination of $K_p = 150$, $K_i = 100$, $K_d = 1000$, $I_sup = 1$, and $V_sup = 1.5$ was chosen for the subsequent larva touch experiments since it yielded the fastest dynamic response with a short rise time of 612 ms and an acceptable overshoot of 20%. Fig. 5(B) shows the tracking response of a multi-step force with the five controller parameters selected above.

B. Larva Stimulation and Fluorescence Imaging

After the force controller was optimized, larva stimulation and fluorescence imaging experiments were performed. The two microrobots moved the larva samples and the pipette at a speed of 500 μm/s during closed-loop position control, and the touch force was accurately controlled to be 5 mN. The whole manipulation process of a single larva (from positioning the larva into the field of view to completion of touching and imaging) took 15 s, yielding a speed of 4 larvae/minutes. 40 samples (10 arrays) have been tested, out of which 37 samples were successfully touched and imaged, with a success rate of 92.5%. The reason for the three failures was that the head of a larva was sometimes tilted, but the image processing algorithm assumed that the larva's spine is strictly horizontal. This caused the pipette tip to miss the ideal touch location and thus invalidated the fluorescence imaging data. This failure mode can be avoid by changing the imaging processing algorithm to extract the larva spine and determine the touch location along it.

Figs. 6(A)(B) show the fluorescent photos taken online before and after a 5 mN touch. The glowing spots in the larva body are the GFP-expressing Tutl-positive neurons. Three groups of Tutl-positive neurons (the ones in area 1, area 2, and area 3) were selected for quantitative analysis, and the average fluorescence intensity values of these areas were measured off line as shown in Fig. 6(C). For all these three groups of neurons, their GFP expressions were significantly changed after robotic touching. This preliminary results demonstrate the effectiveness of the robotic system for simultaneous mechanical stimulation and fluorescence imaging of Drosophila larvae.

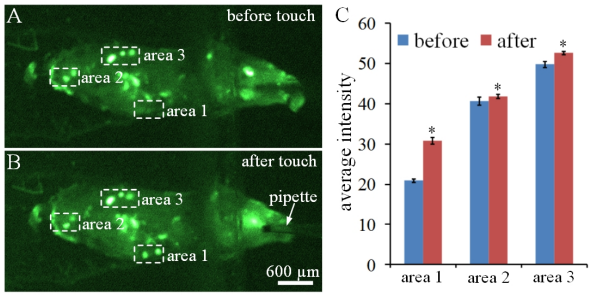

Fig. 6. Fluorescence imaging results measured before and after robotic touching at the level of 5 mN. (A)(B) Fluorescent images of a Drosophila larva taken (A) before and (B) after the 5 mN touch. (C) Quantitative data of the average fluorescence intensity values of area 1-3 measured before and after touching. *p <0.05 as compared to the intensity values measured before touching.

IV. CONCLUSIONS

An automated robotic micromanipulation system with force-control capability was developed for mechanotransduction studies of *Drosophila* larvae. Using a PDMS immobilization device, *Drosophila* larvae were securely immobilized into an array for robotic manipulation. An image processing algorithm was developed for recognizing the pipette tip and the touch location on the larva, providing vision feedback for closed-loop position control. A MEMS force sensor, mounted with a glass pipette, was controlled to touch a larva, during which the touch force was regulated using a closed-loop controller. The force controller was optimized to provide excellent dynamic response and reliable force-regulated touching. The fluorescence imagining results proved the feasibility of using the system for studying transmission responses of Tutl-positive neurons to mechanical stimuli.

REFERENCES

[1] K. Kim, X. Liu, Y. Zhang, and Y. Sun, "Nanonewton force-controlled manipulation of biological cells using a monolithic mems microgripper with two-axis force feedback," *Journal of micromechanics and microengineering*, vol. 18, no. 5, p. 055013, 2008.

[2] W. H. Wang, X. Y. Liu, and Y. Sun, "High-throughput automated injection of individual biological cells," *Automation Science and Engineering, IEEE Transactions on*, vol. 6, no. 2, pp. 209–219, 2009.

[3] X. Liu, Z. Lu, and Y. Sun, "Orientation control of biological cells under inverted microscopy," *Mechatronics, IEEE/ASME Transactions on*, vol. 16, no. 5, pp. 918–924, 2011.

[4] X. Liu, R. Fernandes, M. Gertsenstein, A. Perumalsamy, I. Lai, M. Chi, K. H. Moley, E. Greenblatt, I. Jurisica, R. F. Casper, *et al.*, "Automated microinjection of recombinant bcl-x into mouse zygotes enhances embryo development," *PloS ONE*, vol. 6, no. 7, p. e21687, 2011.

[5] X. Liu, J. Shi, Z. Zong, K.-T. Wan, and Y. Sun, "Elastic and viscoelastic characterization of mouse oocytes using micropipette indentation," *Annals of Biomedical Eng.*, vol. 40, no. 10, pp. 2122–2130, 2012.

[6] Z. Lu, P. C. Chen, and W. Lin, "Force sensing and control in micromanipulation," *Systems, Man, and Cybernetics, Part C: Applications and Reviews, IEEE Transactions on*, vol. 36, no. 6, pp. 713–724, 2006.

[7] X. Liu, Y. Sun, W. Wang, and B. M. Lansdorp, "Vision-based cellular force measurement using an elastic microfabricated device," *Journal of Micromechanics and Microengineering*, vol. 17, no. 7, p. 1281, 2007.

[8] M. Girot, M. Boukallel, and S. Régnier, "A microforce and nanoforce biomicroscope device for in vitro mechanotransduction investigation," *IEEE Transactions on Instrumentation and Measurement*, vol. 57, no. 11, p. 2532, 2008.

[9] G. G. Ernstrom and M. Chalfie, "Genetics of sensory mechanotransduction," *Annual Review of Genetics*, vol. 36, no. 1, pp. 411–453, 2002.

[10] Y. Zhou, S. Cameron, W.-T. Chang, Y. Rao, *et al.*, "Control of directional change after mechanical stimulation in drosophila," *Molecular Brain*, vol. 5, no. 1, p. 39, 2012.

[11] M. Ghannad-Rezaie, X. Wang, B. Mishra, C. Collins, and N. Chronis, "Microfluidic chips for in vivo imaging of cellular responses to neural injury in drosophila larvae," *PloS ONE*, vol. 7, no. 1, p. e29869, 2012.

[12] N. Otsu, "A threshold selection method from gray-level histograms," *Systems, Man and Cybernetics, IEEE Transactions on*, vol. 9, no. 1, pp. 62–66, 1979.